Imaging of 3D objects with experimental data using orthogonality sampling methods

Thu Le* Dinh-Liem Nguyen* Hayden Schmidt* Trung Truong*

Abstract

This paper is concerned with imaging of 3D scattering objects with experimental data from the Fresnel database. The first goal of the paper is to investigate a modified version of the orthogonality sampling method (OSM) by Harris and Nguyen [SIAM J. Sci. Comput., 42, B72–B737, 2020] for the imaging problem. The advantage of the modified OSM over its original version lies in its applicability to more types of polarization vectors associated with the electromagnetic scattering data. We analyze the modified OSM using the factorization analysis for the far field operator and the Funk-Hecke formula. The second goal is to verify the performance of the modified OSM, the OSM, and the classical factorization method for the 3D Fresnel database. The modified OSM we propose is able to invert the sparse and limited-aperture real data in a fast, simple, and efficient way. It is also shown in the real data verification that the modified OSM performs better than its original version and the factorization method.

Keywords. orthogonality sampling method, 3D experimental data, inverse scattering, Maxwell's equations

AMS subject classification. 35R30, 35R09, 65R20

1 Introduction

We consider the electromagnetic inverse scattering problem that aims to determine the shape and location of 3D objects from far-field measurements. This inverse problem, which is an important problem in inverse scattering theory, has applications in nondestructive testing, radar, and medical imaging. Sampling methods are a major approach for numerically solving the inverse problem. These methods are non-iterative, fast, and use little to no a priori information about the unknown targets. Thanks to these advantages, sampling methods have been extensively studied in the inverse scattering community.

*Department of Mathematics, Kansas State University, Manhattan, KS 66506; (thule@ksu.edu, dlnguyen@ksu.edu, hschmidt18@ksu.edu, trungt@ksu.edu)

The linear sampling method [9] can be considered as the first sampling method, which quickly initiated the development of many other sampling methods including the point source method [30], the factorization method [19], the enclosure method [16], etc. We refer to [3, 10, 22] for more details about sampling methods and their recent developments.

We are interested in the orthogonality sampling method (OSM) which has been studied more recently. It was proposed by Potthast in [31] and has recently received more attention thanks to its efficiency and simplicity. The OSM has also been studied in other works under the name of direct sampling method, see, e.g., [17, 28]. Comparing with classical sampling methods the OSM does not need regularization, its implementation is simpler, and it is more robust against noise in the data. However, its theoretical foundation is far less developed compared with that of the classical sampling methods. The OSM has been studied for the Helmholtz equation in [1, 2, 13]. A recent result for the Maxwell's equations can be found in [15].

The first goal of this paper is to investigate a modified version of the OSM studied in [15]. The advantage of the modified OSM over its original version is that it can be applied to more types of polarization vectors associated with the scattering data. We analyze the modified OSM using the factorization analysis for the far field operator and the Funk-Hecke formula. We investigate the modified OSM for both non-magnetic and magnetic cases for the anisotropic Maxwell's equations. The second goal is to apply the modified OSM, the OSM in [15], and the factorization method to inversion of 3D experimental data from the Fresnel Institute [12]. It is worth mentioning that there have been results on experimental data verification for sampling methods, see, e.g., [2, 8, 18, 23, 29]. Most of these results are for 2D data. The 3D data for two spheres from the Fresnel Institute was studied in [18] with a direct sampling method under a small volume hypothesis of well-separated inhomogeneities. Note that the modified OSM studied in this paper does not require this hypothesis. Some other results on inverting these 3D experimental data can be found in [6, 7, 11, 24, 25] and references therein. Comparing with these results, the modified OSM we study use only co-polarized (PP) datasets at a single frequency. In addition the implementation of the orthogonality sampling methods is simpler, faster, and less expensive than those of the iterative methods studied in the cited papers. However, our methods can only recover geometrical information of the 3D objects. One of the challenges in inverting these 3D real data is that these are sparse data, only the third component of the electric field is measured, and it is measured on a circle. It is shown in the experimental data verification that the modified OSM can successfully invert the real data and performs better than its original version and the classical factorization method.

The paper is organized as follows. In Section 2, we formulate the inverse problem of interest. Section 3 is dedicated to the factorization analysis and the analysis of the modified OSM for the non-magnetic case. The theoretical analysis in Section 3 is extended to the magnetic case in Section 4. Section 5 is dedicated to the experimental data validation and a conclusion is given in Section 6.

2 Inverse electromagnetic scattering

Consider the scattering of time-harmonic electromagnetic waves at wave number $k > 0$ from a possibly anisotropic medium. Let Ω be a bounded Lipschitz domain occupied by the medium. Let ε, μ be respectively the electric permittivity and the magnetic permeability of the medium. Assume $\mathbb{R}^3 \setminus \overline{\Omega}$ is connected and that ε, μ and μ^{-1} are functions in $[L^\infty(\mathbb{R}^3)]^{3\times 3}$. The medium outside of Ω is assumed to be homogeneous. We hence assume that $\varepsilon = \mu = I$ in $\mathbb{R}^3 \setminus \overline{\Omega}$, where I is the 3×3 identity matrix. Denote by $\mathbf{E}_{\text{in}}$ and $\mathbf{E}$ the incident electric field and the total electric field, respectively. Let $\mathbf{u} = \mathbf{E} - \mathbf{E}_{\text{in}}$ be the scattered electric field. We consider the following electromagnetic scattering problem

$$\operatorname{curl}[\mu^{-1}(\mathbf{x})\operatorname{curl}\mathbf{E}] - k^2\varepsilon(\mathbf{x})\mathbf{E} = 0, \quad \text{in } \mathbb{R}^3, \tag{1}$$

$$\operatorname{curl}\mathbf{u} \times \frac{\mathbf{x}}{|\mathbf{x}|} - ik\mathbf{u} = \mathcal{O}(|\mathbf{x}|^{-2}) \quad \text{as } |\mathbf{x}| \to \infty, \tag{2}$$

where the Silver-Müller radiation condition (2) is assumed to hold uniformly with respect to $\mathbf{x}/|\mathbf{x}|$. We refer to [26] for the well-posedness of this scattering problem. To formulate the inverse problem we introduce some notations. Denoting $\widehat{\mathbf{x}} = \mathbf{x}/|\mathbf{x}|$, we define

$$\mathbb{S}^2 = \{\mathbf{x} \in \mathbb{R}^3 : |\mathbf{x}| = 1\} \quad \text{and} \quad \mathbf{L}_t^2(\mathbb{S}^2) = \{\mathbf{v} \in [L^2(\mathbb{S}^2)]^3 : \widehat{\mathbf{x}} \cdot \mathbf{v}(\widehat{\mathbf{x}}) = 0,\ \widehat{\mathbf{x}} \in \mathbb{S}^2\}.$$

We consider the incident plane wave $\mathbf{E}_{\text{in}}(\mathbf{x}, \mathbf{d}, \mathbf{q}) = \mathbf{q}e^{ik\mathbf{x}\cdot\mathbf{d}}$, where $\mathbf{d} \in \mathbb{S}^2$ indicates the direction of the incident propagation and $\mathbf{q} \in \mathbb{R}^3$ is the polarization vector such that $\mathbf{q} \cdot \mathbf{d} = 0$. It's well-known that the corresponding scattered wave $\mathbf{u}(\mathbf{x}, \mathbf{d}, \mathbf{q})$ satisfies

$$\mathbf{u}(\mathbf{x}, \mathbf{d}, \mathbf{q}) = \frac{e^{ik|\mathbf{x}|}}{|\mathbf{x}|}\left(\mathbf{u}^\infty(\widehat{\mathbf{x}}, \mathbf{d}, \mathbf{q}) + O\left(\frac{1}{|\mathbf{x}|^2}\right)\right) \quad \text{as} \quad |\mathbf{x}| \to \infty, \tag{3}$$

uniformly in all directions $\widehat{\mathbf{x}} \in \mathbb{S}^2$. The function $\mathbf{u}^\infty(\widehat{\mathbf{x}}, \mathbf{d}, \mathbf{q})$ belonging to $L_t^2(\mathbb{S}^2)$ for each incident and observation direction is called the far field pattern. We are interested in the following inverse problem.

Inverse problem. Given $\mathbf{u}^\infty(\widehat{\mathbf{x}}, \mathbf{d}, \mathbf{q})$ for all $\widehat{\mathbf{x}}, \mathbf{d} \in \mathbb{S}^2$ for a single wave number, determine the shape and location of the scatterer Ω.

3 Modified OSM: the non-magnetic case $\mu = I$

3.1 Factorization analysis

It is more convenient for the presentation to rewrite (1) for the scattered field $\mathbf{u}$ as

$$\operatorname{curl}\operatorname{curl}\mathbf{u} - k^2\varepsilon(\mathbf{x})\mathbf{u} = k^2 P\mathbf{E}_{\text{in}} \quad \text{in } \mathbb{R}^3, \tag{4}$$

where the contrast P is defined by

$$P := \varepsilon - I.$$

We now define the far field operator $\mathcal{F} : \mathbf{L}_t^2(\mathbb{S}^2) \to \mathbf{L}_t^2(\mathbb{S}^2)$ and Herglotz operator $\mathcal{H} : \mathbf{L}_t^2(\mathbb{S}^2) \to [L^2(\Omega)]^3$ as

$$(\mathcal{F}\mathbf{g})(\widehat{\mathbf{x}}) = \int_{\mathbb{S}^2} \mathbf{u}^\infty(\widehat{\mathbf{x}}, \mathbf{d}, \mathbf{g}(\mathbf{d}))\mathrm{d}s(\mathbf{d}), \quad (\mathcal{H}\mathbf{g})(\mathbf{x}) = \int_{\mathbb{S}^2} \mathbf{g}(\mathbf{d}) e^{ik\mathbf{x}\cdot\mathbf{d}} \mathrm{d}s(\mathbf{d}).$$

It is well known that the Herglotz operator $\mathcal{H}$ is compact and injective. Its adjoint operator $\mathcal{H}^* : [L^2(\Omega)]^3 \to \mathbf{L}_t^2(\mathbb{S}^2)$ of $\mathcal{H}$ is given by

$$\mathcal{H}^*\mathbf{f}(\mathbf{d}) = \mathbf{d} \times \left(\int_\Omega \mathbf{f}(\mathbf{x}) e^{-ik\mathbf{x}\cdot\mathbf{d}} \, \mathrm{d}\mathbf{x} \right) \times \mathbf{d}, \quad \mathbf{d} \in \mathbb{S}^2.$$

The solution operator $\mathcal{G} : [L^2(\Omega)]^3 \to \mathbf{L}_t^2(\mathbb{S}^2)$ is defined by

$$\mathcal{G}\mathbf{f} = \mathbf{v}^\infty \tag{5}$$

where $\mathbf{v} \in H_{\mathrm{loc}}(\mathrm{curl}, \mathbb{R}^3)$ is the solution to (2)–(4) with $\mathbf{E}_{\mathrm{in}} = \mathbf{f}$. It is easy to see that $\mathcal{F}$ has the factorization

$$\mathcal{F} = \mathcal{G}\mathcal{H}. \tag{6}$$

We next define the operator $\mathcal{T} : [L^2(\Omega)]^3 \to [L^2(\Omega)]^3$ as

$$\mathcal{T}\mathbf{f} = k^2 P(\mathbf{f} + \mathbf{v})$$

where again $\mathbf{v} \in H_{\mathrm{loc}}(\mathrm{curl}, \mathbb{R}^3)$ is the solution to (2)–(4) with $\mathbf{E}_{\mathrm{in}} = \mathbf{f}$. The operators defined above are all linear bounded operators, see [20]. It is also known from [20] that the solution operator $\mathcal{G}$ can be factorized as $\mathcal{G} = \mathcal{H}^*\mathcal{T}$. This leads to the following factorization for $\mathcal{F}$ as

$$\mathcal{F} = \mathcal{H}^*\mathcal{T}\mathcal{H}. \tag{7}$$

The following assumption on wave number k is necessary for the further results of the factorization analysis in [20] that are needed for the modified OSM.

Assumption 1. *We assume that the wave number k is not a transmission eigenvalue. That means the only solution to the homogeneous system in $[L^2(\Omega)]^3 \times [L^2(\Omega)]^3$*

$$\begin{aligned} \mathrm{curl}\,\mathrm{curl}\,\mathbf{w} - k^2\varepsilon\,\mathbf{w} &= 0 \quad \text{in } \Omega, \\ \mathrm{curl}\,\mathrm{curl}\,\boldsymbol{v} - k^2\boldsymbol{v} &= 0 \quad \text{in } \Omega, \\ \nu \times \mathbf{w} &= \nu \times \boldsymbol{v} \quad \text{on } \partial\Omega, \\ \nu \times \mathrm{curl}\,\mathbf{w} &= \nu \times \mathrm{curl}\,\boldsymbol{v} \quad \text{on } \partial\Omega, \end{aligned}$$

is the trivial solution.

It is well known that the set of real transmission eigenvalues is at most discrete for a real-valued permittivity, see [5] and the references therein for more details about the transmission eigenvalue problems. The following coercivity result from [14] is important for our theoretical analysis.

Lemma 2. *If either* $\mathrm{Im}\,(P)$ *is uniformly positive definite or there is a constant* $\gamma \geq 0$ *such that* $\mathrm{Re}\,(P) + \gamma \mathrm{Im}\,(P)$ *is uniformly positive definite and* $\mathrm{Im}\,(P)$ *is positive semidefinite, then* $\mathcal{T}$ *is coercive on* $\overline{\mathrm{Range}(\mathcal{H})}$.

We close this section with an important lemma for the analysis of the imaging functional defined in the next section.

Lemma 3. *There exists a positive constant* σ *such that*

$$|(\mathcal{F}\mathbf{g}, \mathbf{g})| \geq \sigma \|\mathcal{H}\mathbf{g}\|^2, \quad \textit{for all } \mathbf{g} \in \mathbf{L}_t^2(\mathbb{S}^2).$$

Proof. Using the factorization of $\mathcal{F}$ in (21) and the coercive property of $\mathcal{T}$ we obtain

$$|(\mathcal{F}\mathbf{g}, \mathbf{g})| = |(\mathcal{H}^*\mathcal{T}\mathcal{H}\mathbf{g}, \mathbf{g})| = |(\mathcal{T}\mathcal{H}\mathbf{g}, \mathcal{H}\mathbf{g})| \geq \sigma \|\mathcal{H}\mathbf{g}\|^2.$$

This completes the proof. □

3.2 The imaging functional and its properties

Let $\mathbf{y}_s$ be the sampling points in the imaging process and $\mathbf{p} \in \mathbb{R}^3$ is a fixed nonzero vector. We define the imaging functional $\mathcal{I}_{MOSM}$ for the modified OSM as

$$\mathcal{I}_{MOSM}(\mathbf{y}_s) := \int_{\mathbb{S}^2} \left| \int_{\mathbb{S}^2} \mathbf{u}^\infty(\widehat{\mathbf{x}}, \mathbf{d}, \mathbf{h}(\mathbf{d}))\, e^{-ik\mathbf{d}\cdot\mathbf{y}_s} \mathrm{d}s(\mathbf{d}) \right|^2 \mathrm{d}s(\widehat{\mathbf{x}}), \tag{8}$$

where

$$\mathbf{h}(\mathbf{d}) = \alpha_1 \mathbf{d} \times \mathbf{p} + \alpha_2 (\mathbf{d} \times \mathbf{p}) \times \mathbf{d}$$

with any $\alpha_1, \alpha_2 \in \mathbb{C}$ such that $|\alpha_1|^2 + |\alpha_2|^2 > 0$.

As for the study of the OSM in [15], to analyze the behavior of the imaging functional $\mathcal{I}_{MOSM}$ it is necessary to connect $\mathcal{I}_{MOSM}$ with the far-field operator $\mathcal{F}$. This can be seen in Lemma 4. An advantage of the modified functional is that it allows us to connect to $\mathcal{F}$ directly and naturally, and thus enables the use of polarization vectors $\mathbf{h}(\mathbf{d})$ instead of only $(\mathbf{d} \times \mathbf{p}) \times \mathbf{d}$ as for the imaging functional of the OSM in [15].

Lemma 4. *The imaging functional* $\mathcal{I}_{MOSM}$ *satisfies*

$$\mathcal{I}_{MOSM}(\mathbf{y}_s) = \|\mathcal{F}\varphi_{\mathbf{y}_s}\|^2, \tag{9}$$

where

$$\varphi_{\mathbf{y}_s}(\mathbf{d}) = \mathbf{h}(\mathbf{d}) e^{-ik\mathbf{d}\cdot\mathbf{y}_s}.$$

Proof. Recall that $\mathbf{h}(\mathbf{d}) = \alpha_1 \mathbf{d} \times \mathbf{p} + \alpha_2 (\mathbf{d} \times \mathbf{p}) \times \mathbf{d}$. It implies that $\varphi_{\mathbf{y}_s}(\mathbf{d}) \cdot \mathbf{d} = 0$ for all $\mathbf{d} \in \mathbb{S}^2$, and hence $\varphi_{\mathbf{y}_s} \in \mathbf{L}^2_t(\mathbb{S}^2)$. Now since $\mathbf{u}^\infty(\widehat{\mathbf{x}}, \mathbf{d}, \mathbf{h}(\mathbf{d}))$ is linear in $\mathbf{h}$, we can rewrite the imaging functional as

$$\mathcal{I}_{MOSM}(\mathbf{y}_s) = \int_{\mathbb{S}^2} \left| \int_{\mathbb{S}^2} \mathbf{u}^\infty(\widehat{\mathbf{x}}, \mathbf{d}, \varphi_{\mathbf{y}_s}(\mathbf{d})) \mathrm{d}s(\mathbf{d}) \right|^2 \mathrm{d}s(\widehat{\mathbf{x}}) = \|\mathcal{F}\varphi_{\mathbf{y}_s}\|^2, \tag{10}$$

which completes the proof. □

The following theorem is the main theorem for our analysis for the behavior of the imaging functional $\mathcal{I}_{MOSM}(\mathbf{y}_s)$.

Theorem 5. *For all $\mathbf{y}_s \in \mathbb{R}^3$ the imaging functional satisfies*

$$\mathcal{I}_{MOSM}(\mathbf{y}_s) \leq \|\mathcal{G}\|^2 \left(|\alpha_1|^2 \|W_{\mathbf{y}_s}\|^2 + |\alpha_2|^2 \|V_{\mathbf{y}_s}\|^2 \right),$$

and

$$\mathcal{I}_{MOSM}(\mathbf{y}_s) \geq \frac{\sigma^2}{\|\mathbf{h}\|^2} \left(|\alpha_1|^2 \|W_{\mathbf{y}_s}\|^2 + |\alpha_2|^2 \|V_{\mathbf{y}_s}\|^2 \right)^2 > 0,$$

where $\mathbf{h}$ is given in (8) and σ is the postive constant in Lemma 3,

$$W_{\mathbf{y}_s}(\mathbf{x}) := \widetilde{W}(\mathbf{y}_s - \mathbf{x}), \quad V_{\mathbf{y}_s}(\mathbf{x}) := \widetilde{V}(\mathbf{y}_s - \mathbf{x}), \quad \text{for } \mathbf{x} \in \Omega,$$

with

$$\widetilde{W}(\mathbf{z}) = 4\pi i (\mathbf{z} \times \mathbf{p}) \frac{\cos(k|\mathbf{z}|) - j_0(k|\mathbf{z}|)}{k|\mathbf{z}|^2},$$

$$\widetilde{V}(\mathbf{z}) = -4\pi \frac{\mathbf{p}|\mathbf{z}|^2 - (\mathbf{p} \cdot \mathbf{z})\mathbf{z}}{|\mathbf{z}|^2} j_0(k|\mathbf{z}|) + 12\pi \frac{(\mathbf{p} \cdot \mathbf{z})\mathbf{z} - \frac{1}{3}\mathbf{p}|\mathbf{z}|^2}{k^2|\mathbf{z}|^4} (\cos(k|\mathbf{z}|) - j_0(k|\mathbf{z}|)).$$

Remark 6. *The functions $|\widetilde{W}(\mathbf{z})|^2$ and $|\widetilde{V}(\mathbf{z})|^2$ peak when $|\mathbf{z}| < r$ for small r and decay rapidly when $|\mathbf{z}| > r$, see Figure 1. This implies that $\|W_{\mathbf{y}_s}\|^2 = \int_\Omega |\widetilde{W}(\mathbf{y}_s - \cdot)|^2 \mathrm{d}\mathbf{x}$ and $\|V_{\mathbf{y}_s}\|^2 = \int_\Omega |\widetilde{V}(\mathbf{y}_s - \cdot)|^2 \mathrm{d}\mathbf{x}$ should have large values for $\mathbf{y}_s \in \Omega$ and are significantly small for $\mathbf{y}_s \notin \Omega$, see Figure 2 for an illustration when Ω is a ball. We can also derive the decay rate as*

$$\mathcal{I}_{MOSM}(\mathbf{y}_s) = O\left(\mathrm{dist}(\mathbf{y}_s, \Omega)^{-2} \right) \text{ as } dist(\mathbf{y}_s, \Omega) \to \infty.$$

Theorem 5 shows that $\mathcal{I}_{MOSM}(\mathbf{y}_s)$ should work as an imaging functional for scatterer Ω and it works for all polarizations $\alpha_1 \mathbf{d} \times \mathbf{p} + \alpha_2 (\mathbf{d} \times \mathbf{p}) \times \mathbf{d}$ with $|\alpha_1|^2 + |\alpha_2|^2 > 0$.

Proof. We recall a special form of the Funk-Hecke formula (see [10]) that is important for the proof

$$\int_{\mathbb{S}^2} e^{-ik\mathbf{d}\cdot\mathbf{z}} \, \mathrm{d}s(\mathbf{d}) = 4\pi j_0(k|\mathbf{z}|), \tag{11}$$

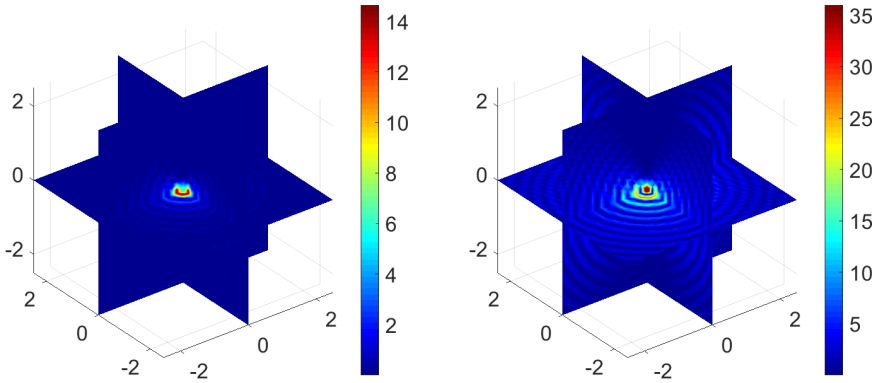

(a) $|\widetilde{W}|^2$ (b) $|\widetilde{V}|^2$

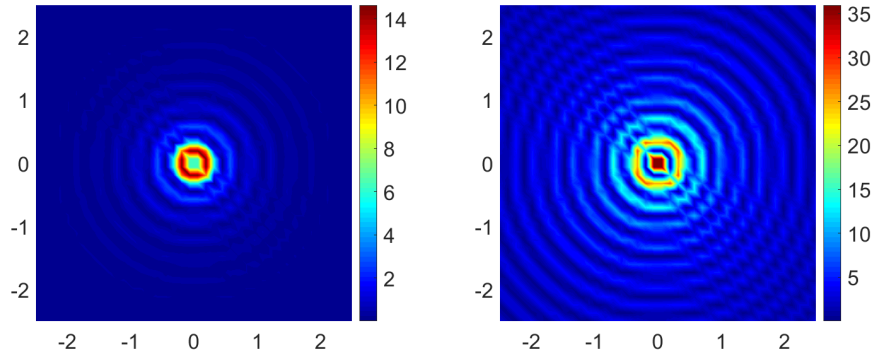

(c) Top view of (a) (d) Top view of (b)

Figure 1: An illustration of $|\widetilde{W}|^2$ and $|\widetilde{V}|^2$ for $\mathbf{z} \in [-2.5, 2.5]^3$, $k = 10$, $\mathbf{p} = (0, 0, 1)^\top$.

where $j_0(t) = \sin(t)/t$ is the first kind spherical Bessel function of order 0.

Using this integral formula we can calculate that

$$\int_{\mathbb{S}^2} \mathbf{d} \times \mathbf{p}\, e^{-ik\mathbf{d}\cdot\mathbf{z}} \mathrm{d}s(\mathbf{d}) = \frac{4\pi i}{k} \mathrm{curl}_{\mathbf{z}}(\mathbf{p} j_0(k|\mathbf{z}|)) = \widetilde{W}(\mathbf{z}), \tag{12}$$

$$\int_{\mathbb{S}^2} (\mathbf{d} \times \mathbf{p}) \times \mathbf{d}\, e^{-ik\mathbf{d}\cdot\mathbf{z}} \mathrm{d}s(\mathbf{d}) = -\frac{4\pi}{k^2} \mathrm{curl}^2_{\mathbf{z}}(\mathbf{p} j_0(k|\mathbf{z}|)) = \widetilde{V}(\mathbf{z}),$$

where

$$\widetilde{W}(\mathbf{z}) = 4\pi i (\mathbf{z} \times \mathbf{p}) \frac{\cos(k|\mathbf{z}|) - j_0(k|\mathbf{z}|)}{k|\mathbf{z}|^2}, \tag{13}$$

$$\widetilde{V}(\mathbf{z}) = -4\pi \frac{\mathbf{p}|\mathbf{z}|^2 - (\mathbf{p}\cdot\mathbf{z})\mathbf{z}}{|\mathbf{z}|^2} j_0(k|\mathbf{z}|) + 12\pi \frac{(\mathbf{p}\cdot\mathbf{z})\mathbf{z} - \frac{1}{3}\mathbf{p}|\mathbf{z}|^2}{k^2|\mathbf{z}|^4} (\cos(k|\mathbf{z}|) - j_0(k|\mathbf{z}|)). \tag{14}$$

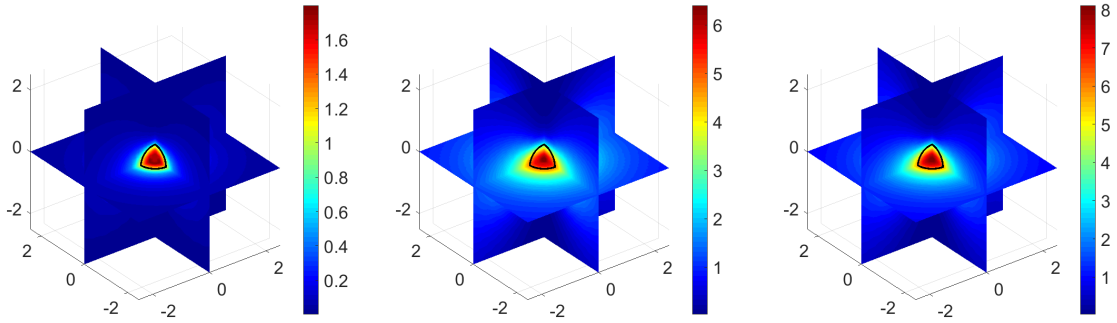

(a) $\|W_{\mathbf{y}_s}\|^2$ (b) $\|V_{\mathbf{y}_s}\|^2$ (c) $\|H_{\mathbf{y}_s}\|^2$

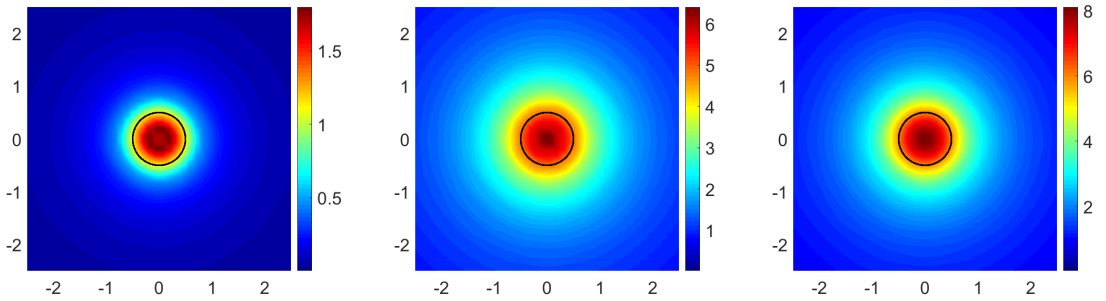

(d) Top view of (a) (e) Top view of (b) (f) Top view of (c)

Figure 2: An illustration of $\|W_{\mathbf{y}_s}\|^2$, $\|V_{\mathbf{y}_s}\|^2$, and $\|H_{\mathbf{y}_s}\|^2$ for $\mathbf{y}_s \in [-2.5, 2.5]^3$, $\Omega = \{\mathbf{z} \in \mathbb{R}^3 : |\mathbf{z}| \leq 0.5\}$, $k = 10$, $\alpha_1 = \alpha_2 = 1$, $\mathbf{p} = (0, 0, 1)^\top$.

It can be checked that $\widetilde{W}(\mathbf{z}) = \widetilde{V}(\mathbf{z}) = O(1/|\mathbf{z}|)$ as $|\mathbf{z}| \to \infty$. We define

$$W_{\mathbf{y}_s}(\mathbf{x}) = \widetilde{W}(\mathbf{y}_s - \mathbf{x}), \quad V_{\mathbf{y}_s}(\mathbf{x}) = \widetilde{V}(\mathbf{y}_s - \mathbf{x}). \tag{15}$$

Recall that $\varphi_{\mathbf{y}_s}(\mathbf{d}) = \mathbf{h}(\mathbf{d})e^{-ik\mathbf{d}\cdot\mathbf{y}_s}$. It follows from the definition of the Herglotz operator $\mathcal{H}$ that

$$\mathcal{H}\varphi_{\mathbf{y}_s}(\mathbf{x}) = \alpha_1 W_{\mathbf{y}_s}(\mathbf{x}) + \alpha_2 V_{\mathbf{y}_s}(\mathbf{x}), \quad \mathbf{x} \in \Omega.$$

Now rewriting

$$\begin{aligned}\widetilde{V}(\mathbf{z}) = \mathbf{z}\left(4\pi\frac{(\mathbf{p}\cdot\mathbf{z})}{|\mathbf{z}|^2}j_0(k|\mathbf{z}|) + 12\pi\frac{(\mathbf{p}\cdot\mathbf{z})}{k^2|\mathbf{z}|^4}(\cos(k|\mathbf{z}|) - j_0(k|\mathbf{z}|))\right)\\ - \mathbf{p}\left(4\pi + 4\pi\frac{\cos(k|\mathbf{z}|) - j_0(k|\mathbf{z}|)}{k^2|\mathbf{z}|^2}\right),\end{aligned}$$

we can deduce that

$$\overline{\widetilde{V}(\mathbf{z})} \cdot \widetilde{W}(\mathbf{z}) = 0, \quad \text{for all } \mathbf{z} \in \mathbb{R}^3.$$

Therefore

$$\|\mathcal{H}\varphi_{\mathbf{y}_s}\|^2 = |\alpha_1|^2 \|W_{\mathbf{y}_s}\|^2 + |\alpha_2|^2 \|V_{\mathbf{y}_s}\|^2. \tag{16}$$

Now consider $\mathbf{y}_s \notin \Omega$. We have from Lemma 4 and the factorization (6) that

$$\mathcal{I}_{MOSM}(\mathbf{y}_s) = \|\mathcal{F}\varphi_{\mathbf{y}_s}\|^2 \leq \|\mathcal{G}\|^2 \|\mathcal{H}\varphi_{\mathbf{y}_s}\|^2,$$

which implies the first estimate of the theorem.

From Lemma 3 and the Cauchy-Schwartz inequality we have

$$\|\mathcal{F}\varphi_{\mathbf{y}_s}\| \|\varphi_{\mathbf{y}_s}\| \geq |(\mathcal{F}\varphi_{\mathbf{y}_s}, \varphi_{\mathbf{y}_s})| \geq \sigma \|\mathcal{H}\varphi_{\mathbf{y}_s}\|^2.$$

Thus using (10) and (16) it follows

$$\mathcal{I}_{MOSM}(\mathbf{y}_s) \geq \frac{\sigma^2}{\|\mathbf{h}\|^2} (|\alpha_1|^2 \|W_{\mathbf{y}_s}\|^2 + |\alpha_2|^2 \|V_{\mathbf{y}_s}\|^2)^2, \quad \text{for all } \mathbf{y}_s \in \Omega.$$

This lower bound is strictly positive thanks to the injectivity of $\mathcal{H}$ and the relation (16). This completes the proof of the theorem. □

Now recall that the imaging functional of the OSM studied in [15] is defined by

$$\mathcal{I}_{OSM}(\mathbf{y}_s) = \int_{\mathbb{S}^2} \left| \int_{\mathbb{S}^2} \mathbf{u}^\infty(\widehat{\mathbf{x}}, \mathbf{d})((\mathbf{d} \times \mathbf{p}) \times \mathbf{d}) \cdot (\widehat{\mathbf{x}} \times \mathbf{p}) \times \widehat{\mathbf{x}}\, e^{ik\widehat{\mathbf{x}} \cdot \mathbf{y}_s} \mathrm{d}s(\widehat{\mathbf{x}}) \right|^2 \mathrm{d}s(\mathbf{d}),$$

where $\mathbf{p} \in \mathbb{R}^3$ is some polarization vector. We provide a relation between the imaging functionals $\mathcal{I}_{MOSM}$ and $\mathcal{I}_{OSM}$ in the case $\alpha_1 = 0$.

Corollary 7. *When $\alpha_1 = 0$, the two imaging functionals satisfy*

$$\mathcal{I}_{OSM}(\mathbf{y}_s) \leq \frac{|\mathbf{p}|^2}{|\alpha_2|^2} \mathcal{I}_{MOSM}(\mathbf{y}_s), \quad \textit{for all } \mathbf{y}_s \in \mathbb{R}^3.$$

Proof. The proof follows from a combination of Lemma 4, Lemma 5 in [15], and the Cauchy-Schwarz inequality. □

This method is stable with respect to noise in the data. Indeed, assume that we only know the far field data $\mathcal{F}$ up to a perturbation $\mathcal{F}_\delta$ such that

$$\|\mathcal{F} - \mathcal{F}_\delta\| \leq \delta \|\mathcal{F}\|$$

for some $\delta > 0$. Denoting by $\mathcal{I}_{MOSM,\delta}$ the imaging functional corresponding to $\mathcal{F}_\delta$, we can derive the following stability estimate as in Theorem 7 in [15]

Theorem 8. *The imaging functionals $\mathcal{I}_{MOSM}$ and $\mathcal{I}_{MOSM,\delta}$ satisfy*

$$|\mathcal{I}_{MOSM}(\mathbf{y}_s) - \mathcal{I}_{MOSM,\delta}(\mathbf{y}_s)| \leq (\delta^2 + 2\delta) \|\mathcal{F}\|^2 \|\mathbf{h}\|^2, \quad \textit{for all } \mathbf{y}_s \in \mathbb{R}^3.$$

4 Modified OSM: the magnetic case $\mu = \mu(\mathbf{x})$

As in the previous section, we first study the factorization analysis for the far field operator and then analyze the imaging functional for the modified OSM.

4.1 Factorization analysis

Recall that $P = \varepsilon - I$. Let $Q = I - \mu^{-1}$. We rewrite the scattering problem for the scattered field $\mathbf{u}$ as

$$\operatorname{curl}\operatorname{curl}\mathbf{u} - k^2\mathbf{u} = k^2 P(\mathbf{f}+\mathbf{u}) + \operatorname{curl}\left[Q(\mathbf{g}+\operatorname{curl}\mathbf{u})\right], \quad \text{in } \mathbb{R}^3, \tag{17}$$

$$\operatorname{curl}\mathbf{u}\times\frac{\mathbf{x}}{|\mathbf{x}|} - ik\mathbf{u} = \mathcal{O}(|\mathbf{x}|^{-2}) \text{ as } |\mathbf{x}|\to\infty. \tag{18}$$

Here the general $(\mathbf{f},\mathbf{g}) \in [L^2(\Omega)]^3 \times [L^2(\Omega)]^3$ in the right hand side is convenient for our presentation. If $(\mathbf{f},\mathbf{g}) = (\mathbf{E}_{in}, \operatorname{curl}\mathbf{E}_{in})$, we have the original scattering problem. The following assumption is important for the analysis in this section.

Assumption 9. *Assume that there exist $C_1, C_2 > 0$ such that for all $\mathbf{z} \in \mathbb{C}^3$*

$$\operatorname{Im}(Q\mathbf{z}\cdot\bar{\mathbf{z}}) \geq C_1|\mathbf{z}|^2, \qquad \operatorname{Im}(P\mathbf{z}\cdot\bar{\mathbf{z}}) \geq C_2|\mathbf{z}|^2$$

almost everywhere in Ω.

Note that unlike in the non-magnetic case this assumption excludes the transmission eigenvalues in the scattering problem. We now define the far field operator $\mathcal{F} : \mathbf{L}_t^2(\mathbb{S}^2) \to \mathbf{L}_t^2(\mathbb{S}^2)$ and the solution operator $\mathcal{G} : [L^2(\Omega)]^3 \times [L^2(\Omega)]^3 \to \mathbf{L}_t^2(\mathbb{S}^2)$

$$(\mathcal{F}\mathbf{p})(\widehat{\mathbf{x}}) = \int_{\mathbb{S}^2} \mathbf{u}^\infty(\widehat{\mathbf{x}},\mathbf{d},\mathbf{p}(\mathbf{d}))\mathrm{d}s(\mathbf{d}), \quad \mathcal{G}(\mathbf{f},\mathbf{g}) = \mathbf{u}^\infty$$

where $\mathbf{u}^\infty$ is the far field pattern of $\mathbf{u}$ satisfying (2) and

$$\begin{aligned}&\int_{\mathbb{R}^2} \operatorname{curl}\mathbf{u}\cdot\operatorname{curl}\overline{\mathbf{v}} - k^2\mathbf{u}\cdot\overline{\mathbf{v}}\,\mathrm{d}\mathbf{x}\\ &= \int_\Omega [k^2P(\mathbf{u}+\mathbf{f})]\cdot\overline{\mathbf{v}}\,\mathrm{d}\mathbf{x} + \int_\Omega Q(\operatorname{curl}\mathbf{u}+\mathbf{g})\cdot\operatorname{curl}\overline{\mathbf{v}}\,\mathrm{d}\mathbf{x},\end{aligned} \tag{19}$$

for all $\mathbf{v} \in H(\operatorname{curl},\mathbb{R}^3)$ with compact support. It is known in [21] that equation (19) is equivalent to the integro-differential equation

$$\mathbf{u}(\mathbf{x}) = (k^2+\nabla\operatorname{div})\int_\Omega \Phi(\mathbf{x},\mathbf{y})[P(\mathbf{u}+\mathbf{f})](\mathbf{y})\mathrm{d}\mathbf{y} + \operatorname{curl}\int_\Omega \Phi(\mathbf{x},\mathbf{y})[Q(\operatorname{curl}\mathbf{u}+\mathbf{g})](\mathbf{y})\mathrm{d}\mathbf{y},$$

where $\Phi(\mathbf{x},\mathbf{y}) = \exp(ik|\mathbf{x}-\mathbf{y}|)/(4\pi|\mathbf{x}-\mathbf{y}|)$ is the free-space Green function of the scalar Helmholtz equation. Let $\mathcal{H}_{1,2} : \mathbf{L}^2_t(\mathbb{S}^2) \to [L^2(\Omega)]^3$ be defined by

$$(\mathcal{H}_1\mathbf{p})(\mathbf{y}) = \int_{\mathbb{S}^2} \mathbf{p}(\mathbf{d}) e^{ik\mathbf{d}\cdot\mathbf{y}} \mathrm{d}s(\mathbf{d}) \quad \text{and} \quad \mathcal{H}_2\mathbf{p} = \operatorname{curl} \mathcal{H}_1\mathbf{p}.$$

The Herglotz operator $\mathcal{H} : \mathbf{L}^2_t(\mathbb{S}^2) \to [L^2(\Omega)]^3 \times [L^2(\Omega)]^3$ in the magnetic case is defined by

$$\mathcal{H}\mathbf{p} = (\mathcal{H}_1\mathbf{p}, \mathcal{H}_2\mathbf{p})^\top. \tag{20}$$

The adjoint operators $\mathcal{H}^*_{1,2}$ of $\mathcal{H}_{1,2}$ are given by $\mathcal{H}^*_{1,2} : [L^2(\Omega)]^3 \to \mathbf{L}^2_t(\mathbb{S}^2)$

$$(\mathcal{H}^*_1\mathbf{g})(\mathbf{d}) = \mathbf{d} \times \int_\Omega \mathbf{g}(\mathbf{y}) e^{-ik\mathbf{d}\cdot\mathbf{y}} \mathrm{d}\mathbf{y} \times \mathbf{d}, \quad (\mathcal{H}^*_2\mathbf{g})(\mathbf{d}) = ik\mathbf{d} \times \int_\Omega \mathbf{g}(\mathbf{y}) e^{-ik\mathbf{d}\cdot\mathbf{y}} \mathrm{d}\mathbf{y}.$$

Then the adjoint operator $\mathcal{H}^* : [L^2(\Omega)]^3 \times [L^2(\Omega)]^3 \to \mathbf{L}^2_t(\mathbb{S}^2)$ of the Herglotz operator is given by

$$\mathcal{H}^*(\mathbf{f},\mathbf{g}) = \mathcal{H}^*_1\mathbf{f} + \mathcal{H}^*_2\mathbf{g}.$$

As in the non-magnetic case we can factorize the far field operator as

$$\mathcal{F} = \mathcal{G}\mathcal{H}. \tag{21}$$

For $(\mathbf{f},\mathbf{g})^\top \in [L^2(\Omega)]^3 \times [L^2(\Omega)]^3$, the middle operator $\mathcal{T} : [L^2(\Omega)]^3 \times [L^2(\Omega)]^3 \to [L^2(\Omega)]^3 \times [L^2(\Omega)]^3$ is defined by

$$\mathcal{T}(\mathbf{f},\mathbf{g}) := (k^2 P(\mathbf{u}+\mathbf{f}), Q(\operatorname{curl}\mathbf{u} + \mathbf{g}))^\top \tag{22}$$

where $\mathbf{u}$ is the solution to (19) with $(\mathbf{f},\mathbf{g})$ on the right hand side.

Lemma 10. *The operator $\mathcal{T}$ defined by* (22) *is a linear bounded operator on $[L^2(\Omega)]^3 \times [L^2(\Omega)]^3$.*

Proof. Consider $(\widetilde{\mathbf{f}},\widetilde{\mathbf{g}}) \in [L^2(\Omega)]^3 \times [L^2(\Omega)]^3$ and let $\widetilde{\mathbf{u}}$ be the solution with this right hand side in (19). Then

$$\mathcal{T}(\widetilde{\mathbf{f}},\widetilde{\mathbf{g}}) = (k^2 P(\widetilde{\mathbf{u}}+\widetilde{\mathbf{f}}), Q(\operatorname{curl}\widetilde{\mathbf{u}} + \widetilde{\mathbf{g}}))^\top.$$

Therefore for any $a, b \in \mathbb{C}$ we obtain

$$\begin{aligned} a\mathcal{T}(\mathbf{f},\mathbf{g}) + b\mathcal{T}(\widetilde{\mathbf{f}},\widetilde{\mathbf{g}}) &= (k^2 P(b\widetilde{\mathbf{u}} + a\mathbf{u} + b\widetilde{\mathbf{f}} + a\mathbf{f}), Q(b\operatorname{curl}\widetilde{\mathbf{u}} + a\operatorname{curl}\mathbf{u} + b\widetilde{\mathbf{g}} + a\mathbf{g}))^\top \\ &= \mathcal{T}(a(\mathbf{f},\mathbf{g}) + b(\widetilde{\mathbf{f}},\widetilde{\mathbf{g}})), \end{aligned}$$

thanks to linearity of the problem (19).

For $(\mathbf{f},\mathbf{g}) \in [L^2(\Omega)]^3 \times [L^2(\Omega)]^3$, since (19) is well-posed, there exists a constant $C > 0$ such that

$$\|\mathbf{u}\|_{H(\operatorname{curl},\Omega)} \le C\|(\mathbf{f},\mathbf{g})\|.$$

We can deduce the boundedness of T from the following additional estimates

$$\|P(\mathbf{u}+\mathbf{f})\| \le \||P|_F\|_{L^\infty}(\|\mathbf{u}\|_{H(\mathrm{curl},\Omega)} + \|\mathbf{f}\|),$$
$$\|Q(\mathrm{curl}\,\mathbf{u}+\mathbf{g})\| \le \||Q|_F\|_{L^\infty}(\|\mathbf{u}\|_{H(\mathrm{curl},\Omega)} + \|\mathbf{g}\|),$$

where $|\cdot|_F$ is the Frobenius matrix norm. This completes the proof. □

Lemma 11. *The far field operator $\mathcal{F}$ can be factorized as*

$$\mathcal{F} = \mathcal{H}^*\mathcal{T}\mathcal{H}.$$

Proof. Since $\mathcal{F} = \mathcal{G}\mathcal{H}$, it is sufficient to show that $\mathcal{G} = \mathcal{H}^*\mathcal{T}$. We have

$$\mathcal{H}^*\mathcal{T}(\mathbf{f},\mathbf{g}) = \widehat{\mathbf{x}} \times \int_\Omega k^2[P(\mathbf{u}+\mathbf{f})](\mathbf{y})e^{-ik\widehat{\mathbf{x}}\cdot\mathbf{y}}\mathrm{d}\mathbf{y} \times \widehat{\mathbf{x}} + ik\widehat{\mathbf{x}} \times \int_\Omega [Q(\mathrm{curl}\,\mathbf{u}+\mathbf{g})](\mathbf{y})e^{-ik\widehat{\mathbf{x}}\cdot\mathbf{y}}\mathrm{d}\mathbf{y}.$$

It is known that (see, e.g., [27]) the right hand side of the above equation is the far field pattern of the scattered field $\mathbf{u}$ given by

$$\mathbf{u}(\mathbf{x}) = (k^2 + \nabla\mathrm{div}) \int_\Omega \Phi(\mathbf{x},\mathbf{y})[P(\mathbf{u}+\mathbf{f})](\mathbf{y})\mathrm{d}\mathbf{y} + \mathrm{curl} \int_\Omega \Phi(\mathbf{x},\mathbf{y})[Q(\mathrm{curl}\,\mathbf{u}+\mathbf{g})](\mathbf{y})\mathrm{d}\mathbf{y}.$$

This implies that $\mathcal{H}^*\mathcal{T}(\mathbf{f},\mathbf{g}) = \mathbf{u}^\infty = \mathcal{G}(\mathbf{f},\mathbf{g})$. Therefore, $\mathcal{G} = \mathcal{H}^*\mathcal{T}$. □

For the convenience of the presentation of the proof of the following theorem we will use $(\cdot,\cdot)$ and $\|\cdot\|$ indistinctively for the inner product and norm of $[L^2(\Omega)]^3$ and $[L^2(\Omega)]^3 \times [L^2(\Omega)]^3$.

Lemma 12. *There exists $\gamma > 0$ such that*

$$(\mathrm{Im}\,\mathcal{T}(\mathbf{f},\mathbf{g}),(\mathbf{f},\mathbf{g})) \ge \gamma\|(\mathbf{f},\mathbf{g})\|^2 \tag{23}$$

for all $(\mathbf{f},\mathbf{g}) \in \mathrm{Range}(\mathcal{H})$.

Proof. Denote $\mathbf{h}_1 = \mathbf{g} + \mathrm{curl}\,\mathbf{u}$, $\mathbf{h}_2 = \mathbf{f} + \mathbf{u}$. We have

$$\begin{aligned}(\mathcal{T}(\mathbf{f},\mathbf{g}),(\mathbf{f},\mathbf{g})) &= \int_\Omega Q\mathbf{h}_1 \cdot (\overline{\mathbf{h}}_1 - \mathrm{curl}\,\overline{\mathbf{u}})\,\mathrm{d}\mathbf{x} + \int_\Omega k^2 P\mathbf{h}_2 \cdot (\overline{\mathbf{h}}_2 - \overline{\mathbf{u}})\,\mathrm{d}\mathbf{x} \\ &= (Q\mathbf{h}_1,\mathbf{h}_1) + k^2(P\mathbf{h}_2,\mathbf{h}_2) - (Q\mathbf{h}_1,\mathrm{curl}\,\mathbf{u}) - k^2(P\mathbf{h}_2,\mathbf{u}). \end{aligned} \tag{24}$$

From Assumption 9 we obtain that

$$\mathrm{Im}\,(Q\mathbf{h}_1,\mathbf{h}_1)) + k^2\mathrm{Im}\,(P\mathbf{h}_2,\mathbf{h}_2) \ge C_1\|\mathbf{h}_1\|^2 + k^2C_2\|\mathbf{h}_2\|^2.$$

We now estimate the imaginary parts of the last two terms in the right hand side of (24). Since $\mathbf{u}$ is the radiating solution to (19) we have

$$\int_{\mathbb{R}^3} (\mathrm{curl}\,\mathbf{u} \cdot \mathrm{curl}\,\overline{\mathbf{v}} - k^2\mathbf{u}\cdot\overline{\mathbf{v}})\,\mathrm{d}\mathbf{x} = \int_\Omega (Q\mathbf{h}_1 \cdot \mathrm{curl}\,\overline{\mathbf{v}} + k^2 P\mathbf{h}_2 \cdot \overline{\mathbf{v}})\,\mathrm{d}\mathbf{x}. \tag{25}$$

for all $\mathbf{v} \in H(\mathrm{curl}, \mathbb{R}^3)$ with compact support.

Let ρ be a positive constant such that $\overline{\Omega}$ is contained in the ball $\{\mathbf{x} \in \mathbb{R}^3 : |\mathbf{x}| < \rho\}$. Now we take $\mathbf{v} = \phi\mathbf{u}$ in (25) where $\phi \in C^\infty(\mathbb{R}^3)$ is a cut-off function with $\phi = 1$ for $|\mathbf{x}| < \rho$ and $\phi = 0$ for $|\mathbf{x}| \geq 2\rho$, then

$$\int_\Omega Q\mathbf{h}_1 \cdot \mathrm{curl}\,\overline{\mathbf{u}}\,\mathrm{d}\mathbf{x} + k^2 P\mathbf{h}_2 \cdot \overline{\mathbf{u}}\,\mathrm{d}\mathbf{x} = \int_{|x|<\rho} |\mathrm{curl}\,\mathbf{u}|^2 - k^2|\mathbf{u}|^2 \mathrm{d}\mathbf{x} + \int_{\rho<|\mathbf{x}|<2\rho} \mathrm{curl}\,\mathbf{u} \cdot \mathrm{curl}\,(\phi\overline{\mathbf{u}}) - k^2|\mathbf{u}|^2\phi \mathrm{d}\mathbf{x}.$$

Using Stokes' theorem and taking the imaginary part of the right hand side of the above equation we obtain

$$\mathrm{Im} \int_\Omega Q\mathbf{h}_1 \cdot \mathrm{curl}\,\overline{\mathbf{u}}\,\mathrm{d}\mathbf{x} + k^2 P\mathbf{h}_2 \cdot \overline{\mathbf{u}}\,\mathrm{d}\mathbf{x} = \mathrm{Im} \int_{|\mathbf{x}|=\rho} (\widehat{\mathbf{x}} \times \mathrm{curl}\,\mathbf{u}) \cdot \overline{\mathbf{u}}\,\mathrm{d}s(\mathbf{x}).$$

Using the radiation condition (2) and the asymptotic behavior (3) we obtain

$$\lim_{\rho\to\infty} \int_{|\mathbf{x}|=\rho} (\hat{\mathbf{x}} \times \mathrm{curl}\,\mathbf{u}) \cdot \mathbf{u}\,\mathrm{d}s(\mathbf{x}) = -\frac{ik}{(4\pi)^2} \int_{\mathbb{S}^2} |\mathbf{u}^\infty|^2\,\mathrm{d}s(\mathbf{x}).$$

Therefore, we can now estimate the imaginary part of the left hand side of (24) as

$$\mathrm{Im}\,(\mathcal{T}(\mathbf{f},\mathbf{g}),(\mathbf{f},\mathbf{g})) \geq C_1\|\mathbf{h}_1\|^2 + k^2 C_2\|\mathbf{h}_2\|^2 + \frac{k}{(4\pi)^2} \int_{\mathbb{S}^2} |\mathbf{u}^\infty|^2 \mathrm{d}s(\mathbf{x}).$$

From the fact that $(\mathrm{Im}\,\mathcal{T}(\mathbf{f},\mathbf{g}),(\mathbf{f},\mathbf{g})) = \mathrm{Im}\,(\mathcal{T}(\mathbf{f},\mathbf{g}),(\mathbf{f},\mathbf{g}))$ we imply

$$(\mathrm{Im}\,\mathcal{T}(\mathbf{f},\mathbf{g}),(\mathbf{f},\mathbf{g})) \geq C_1\|\mathbf{h}_1\|^2 + k^2 C_2\|\mathbf{h}_2\|^2.$$

Now assume that there is no $\gamma > 0$ such that (23) holds. Then there exists a sequence $\{(\mathbf{f}_j,\mathbf{g}_j)\}_j \subset [L^2(\Omega)]^3 \times [L^2(\Omega)]^3$ such that $\|(\mathbf{f}_j,\mathbf{g}_j)\| = 1$ and

$$(\mathrm{Im}\,\mathcal{T}(\mathbf{f}_j,\mathbf{g}_j),(\mathbf{f}_j,\mathbf{g}_j)) \xrightarrow{j\to\infty} 0.$$

Then it follows $\mathbf{h}_1^j = \mathbf{f}_j + \mathrm{curl}\,\mathbf{u}_j \xrightarrow{j\to\infty} 0$ and $\mathbf{h}_2^j = \mathbf{g}_j + \mathbf{u}_j \xrightarrow{j\to\infty} 0$ in $[L^2(\Omega)]^3$ where $\mathbf{u}_j$ is the solution to

$$\mathbf{u}_j(\mathbf{x}) = (k^2 + \nabla\mathrm{div}) \int_\Omega [P(\mathbf{u}_j + \mathbf{f}_j)]\Phi(\mathbf{x},\mathbf{y})\mathrm{d}\mathbf{y} + \mathrm{curl} \int_\Omega [Q(\mathrm{curl}\,\mathbf{u}_j + \mathbf{g}_j)]\Phi(\mathbf{x},\mathbf{y})\mathrm{d}\mathbf{y}.$$

By the boundedness of the integro-differential operators (see [21]) we obtain

$$\|\mathbf{u}_j\|_{H(\mathrm{curl},\Omega)} \leq C_3\left(\||P|_F\|_{L^\infty}\|\mathbf{g}_j + \mathbf{u}_j\|\right) + C_4\left(\||Q|_F\|_{L^\infty}\|\mathbf{f}_j + \mathrm{curl}\,\mathbf{u}_j\|\right),$$

where C_3 and C_4 are positive constants. Thus $\mathbf{u}_j \xrightarrow{j\to\infty} 0$ in $H(\mathrm{curl},\Omega)$ and therefore $(\mathbf{f}_j,\mathbf{g}_j) \xrightarrow{j\to\infty} 0$ in $[L^2(\Omega)]^3 \times [L^2(\Omega)]^3$. The latter is a contradiction with $\|(\mathbf{f}_j,\mathbf{g}_j)\| = 1$. $\square$

From this coercivity property and the factorization (11), the following lemma, which is similar to Lemma 3, is satisfied in the magnetic case.

Lemma 13. *There exists a positive constant γ such that*

$$|(\mathcal{F}\mathbf{g},\mathbf{g})| \geq \gamma \|\mathcal{H}\mathbf{g}\|^2, \quad \textit{for all } \mathbf{g} \in \mathbf{L}_t^2(\mathbb{S}^2),$$

where $\mathcal{H}$ is defined by (20).

This lemma is again important for the analysis of the imaging functional in the next section.

4.2 The imaging functional and its properties

We consider the same imaging functional $\mathcal{I}_{MOSM}(\mathbf{y}_s)$ as in (8) and this functional also satisfies Lemma 4. We now prove the main theorem for the analysis of the imaging functional in the magnetic case.

Theorem 14. *For all $\mathbf{y}_s \in \mathbb{R}^3$ the imaging functional satisfies*

$$\mathcal{I}_{MOSM}(\mathbf{y}_s) \leq \|\mathcal{G}\|^2 \left[(|\alpha_1|^2 + k^2|\alpha_2|^2)\|W_{\mathbf{y}_s}\|^2 + (k^2|\alpha_1|^2 + |\alpha_2|^2)\|V_{\mathbf{y}_s}\|^2\right],$$

and

$$\mathcal{I}_{MOSM}(\mathbf{y}_s) \geq \frac{\gamma^2}{\|\mathbf{h}\|^2} \left[(|\alpha_1|^2 + k^2|\alpha_2|^2)\|W_{\mathbf{y}_s}\|^2 + (k^2|\alpha_1|^2 + |\alpha_2|^2)\|V_{\mathbf{y}_s}\|^2\right]^2 > 0,$$

where $\mathbf{h}$ is given in (8)*, γ is the postive constant in Lemma 13, and $W_{\mathbf{y}_s}, V_{\mathbf{y}_s}$ are given by* (15).

Proof. Due to the presence of $\mathcal{H}_2$ in the Herglotz operator $\mathcal{H}$ in (20) we need to calculate curl $\int_{\mathbb{S}^2} \mathbf{d}\times\mathbf{p}\, e^{-ik\mathbf{d}\cdot\mathbf{z}} ds(\mathbf{d})$ and curl $\int_{\mathbb{S}^2} (\mathbf{d}\times\mathbf{p})\times\mathbf{d}\, e^{-ik\mathbf{d}\cdot\mathbf{z}} ds(\mathbf{d})$. Using the formula (11) again we derive

$$\text{curl} \int_{\mathbb{S}^2} \mathbf{d}\times\mathbf{p}\, e^{-ik\mathbf{d}\cdot\mathbf{z}} ds(\mathbf{d}) = \frac{4\pi i}{k} \text{curl}_{\mathbf{z}}^2(\mathbf{p} j_0(k|\mathbf{z}|)) = -ik\widetilde{V}(\mathbf{z}),$$

where $\widetilde{V}(\mathbf{z})$ is given by (14). Using (11) and the facts curl $^2 = -\Delta + \nabla\text{div}$, $\Delta j_0(k|\mathbf{z}|) + k^2 j_0(k|\mathbf{z}|) = 0$ we can compute

$$\begin{aligned}\text{curl} \int_{\mathbb{S}^2} (\mathbf{d}\times\mathbf{p})\times\mathbf{d}\, e^{-ik\mathbf{d}\cdot\mathbf{z}} ds(\mathbf{d}) &= -\frac{4\pi}{k^2}\text{curl}_{\mathbf{z}}^3(\mathbf{p} j_0(k|\mathbf{z}|)) = \frac{4\pi}{k^2}\text{curl}_{\mathbf{z}}(\mathbf{p}\Delta j_0(k|\mathbf{z}|)) \\ &= -4\pi \text{curl}_{\mathbf{z}}(\mathbf{p} j_0(k|\mathbf{z}|)) = ik\widetilde{W}(\mathbf{z}),\end{aligned}$$

where $\widetilde{W}(\mathbf{z})$ is given by (13).

Recall $W_{\mathbf{y}_s}$ and $V_{\mathbf{y}_s}$ from (15) and $\mathcal{H}_1\varphi_{\mathbf{y}_s} = \alpha_1 W_{\mathbf{y}_s} + \alpha_2 V_{\mathbf{y}_s}$. Thanks to the above calculations, we derive that

$$\mathcal{H}\varphi_{\mathbf{y}_s} = (\alpha_1 W_{\mathbf{y}_s} + \alpha_2 V_{\mathbf{y}_s}, \alpha_1 ikV_{\mathbf{y}_s} - \alpha_2 ikW_{\mathbf{y}_s})^\top.$$

As proven in the proof of Theorem 5, $W_{\mathbf{y}_s}$ and $V_{\mathbf{y}_s}$ are orthogonal. Therefore, we have

$$\begin{aligned}\|\mathcal{H}\varphi_{\mathbf{y}_s}\|^2 &= \|\alpha_1 W_{\mathbf{y}_s} + \alpha_2 V_{\mathbf{y}_s}\|^2 + \|\alpha_1 ikV_{\mathbf{y}_s} - \alpha_2 ikW_{\mathbf{y}_s}\|^2 \\ &= (|\alpha_1|^2 + k^2|\alpha_2|^2)\|W_{\mathbf{y}_s}\|^2 + (k^2|\alpha_1|^2 + |\alpha_2|^2)\|V_{\mathbf{y}_s}\|^2.\end{aligned}$$

Recall from Lemma 4 that $\mathcal{I}_{MOSM}(\mathbf{y}_s) = \|\mathcal{F}\varphi_{\mathbf{y}_s}\|^2$. As in the proof of Theorem 5 we complete proof of this theorem using the following inequalities

$$\frac{\sigma^2}{\|\mathbf{h}\|^2}\|\mathcal{H}\varphi_{\mathbf{y}_s}\|^4 \leq \|\mathcal{F}\varphi_{\mathbf{y}_s}\|^2 \leq \|\mathcal{G}\|^2\|\mathcal{H}\varphi_{\mathbf{y}_s}\|^2.$$

Here the first inequality follows from the Cauchy-Schwarz inequality and Lemma (13), and the second inequality follows from (21). □

We also have similar properties of the imaging functional as in Corollary 7 and Theorem 8.

5 Experimental data verification

We apply the classical factorization method (FM) [22], the OSM in [15] and the modified OSM to invert the 3D experimental database provided by the Fresnel Institute, France [12]. More precisely, we invert the calibrated co-polarized datasets (TwoSpheres-PP, TwoCubes-PP, Cylinder-PP, CubeSpheres-PP, IsocaSphere-PP) for all the examples in this section. The sampling methods are implemented using the computing software Matlab. We rescale 40 millimeters to be 1 unit of length in our Matlab simulations. From now on we will use scaled lengths in the presentation instead of actual lengths, for example 2 instead of 80 millimeters. The sampling domain is the cube $[-2.5, 2.5]^3$ uniformly divided into $32 \times 32 \times 32$ sampling points. The far-field pattern is computed from the measured scattered field via (3). The distance from the origin to the receivers (and the sources) is 44.9, which is large enough to guarantee a good approximation in (3).

In the experiments the targets are illuminated by 81 incident sources that are located far away, see Figure 3(a) for the distribution of the sources. However, due to technical reasons, the scattered electric field was collected at only 36 points on $\mathbb{S}^2 \cap \{z = 0\}$, see Figure 3(b), and only the third component of the scattered field was measured. This is certainly the main challenge for the sampling methods which typically require full aperture data. When computing the integrals to evaluate the imaging functionals, the points where no data is present are treated as 0. Note that the measured data can be enhanced using the reciprocity property of the far field pattern but here we would like to test the performance of the sampling methods for the original limited-aperture data.

To help the readers understand better our reconstruction results we use the information provided by the Fresnel Institute in [12] to create 3D objects mimicking the true 3D targets used in the experiments. The isovalue used in the 3D isosurface plotting for the case of IsocaSphere is 0.78 (78% of the maximal value of the imaging functionals that are normalized). This isovalue is 0.5 in all of the other cases.

The real data should correspond to the non-magnetic case ($\mu = I$). The analysis of the MOSM in this case requires Assumption 1 about the transmission eigenvalues. Finding these eigenvalues is by far a nontrivial task, see [4]. Thus we can't verify whether the wave numbers used in the real data validation are transmission eigenvalues. However, the chance of having these transmission eigenvalues could be small since it is known that the set of such eigenvalues is at most a discrete set. Furthermore, Assumption 9 may not hold for the real data since the imaginary part of the permittivity ε is probably small and negligible according to [12].

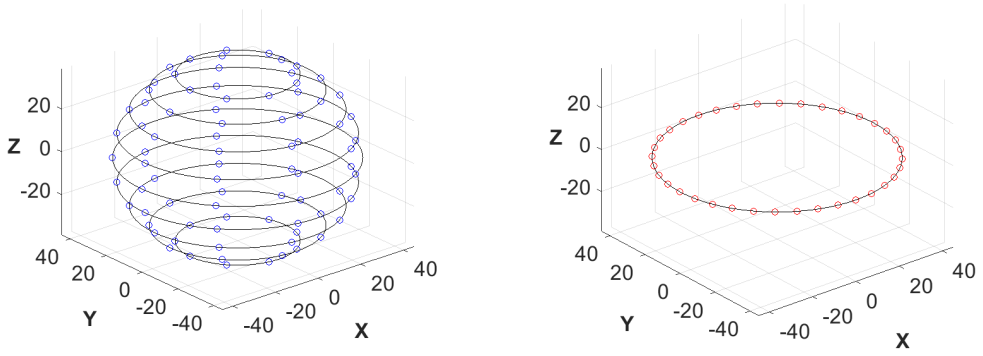

(a) Sources (b) Receivers

Figure 3: The experimental setup for incident sources and data receivers.

TwoSpheres-PP dataset (Figure 4) and Cylinder-PP dataset (Figure 5). For the first two datasets we can see that the OSM seems to be able to reconstruct only information in the (x, y)-plane of the targets. This can be due to the lack of measured data in the z-direction. However, the FM and the MOSM are able to provide more reasonable reconstructions. The FM is able to locate the targets but fails to provide reasonable shapes while the MOSM can not only locate targets but also provide a pretty good shape reconstruction in the case of TwoSpheres-PP dataset. Its result for the Cylinder-PP dataset also looks more reasonable than that of the FM. The cylinder object has the largest volume among all the targets and is challenging to reconstruct, see notice in [12]. Only the data set at 3 GHz gives a reasonable result for this target.

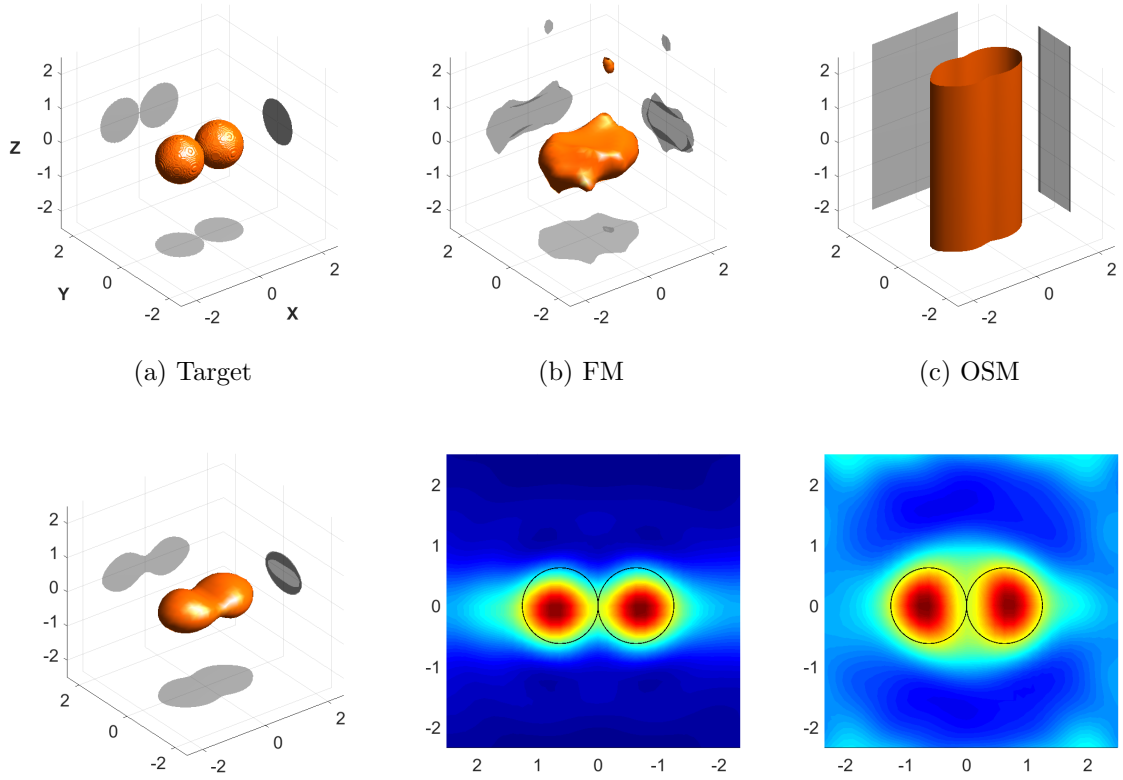

(a) Target (b) FM (c) OSM

(d) MOSM (e) $\mathcal{I}_{MOSM}$ on $\{y = 0\}$ (f) $\mathcal{I}_{MOSM}$ on $\{z = 0\}$

Figure 4: Reconstruction with TwoSpheres-PP dataset at 4 GHz.

TwoCubes-PP dataset (Figure 6), CubeSpheres-PP dataset (Figure 7). For these datasets the OSM provides similar performance as in the first two cases. It fails to reconstruct the z-direction of the targets. The reconstruction results of the FM again can provide the location of the targets. Moreover, the FM can even resolve and provide reasonable size of the two cubes for the TwoCubes-PP dataset, see Figure 3(b). From the reconstruction results of the MOSM we can see that the MOSM are again slightly better than those of the FM. The MOSM can locate the targets and provide more accurate information about the shape of the targets.

IsocaSphere-PP dataset (Figure 8) This is also known as the *Myster* object and is the most complex in the database. It consists of twelve small spheres but not as evenly distributed as those of CubeSpheres-PP dataset. Comparing with the OSM and FM, the MOSM again performs better. The OSM again fails to image the z-direction of the target while the FM can't reconstruct any information for this case. The MOSM can recover the location of the target and provide a rough estimate of the shape of the target in the

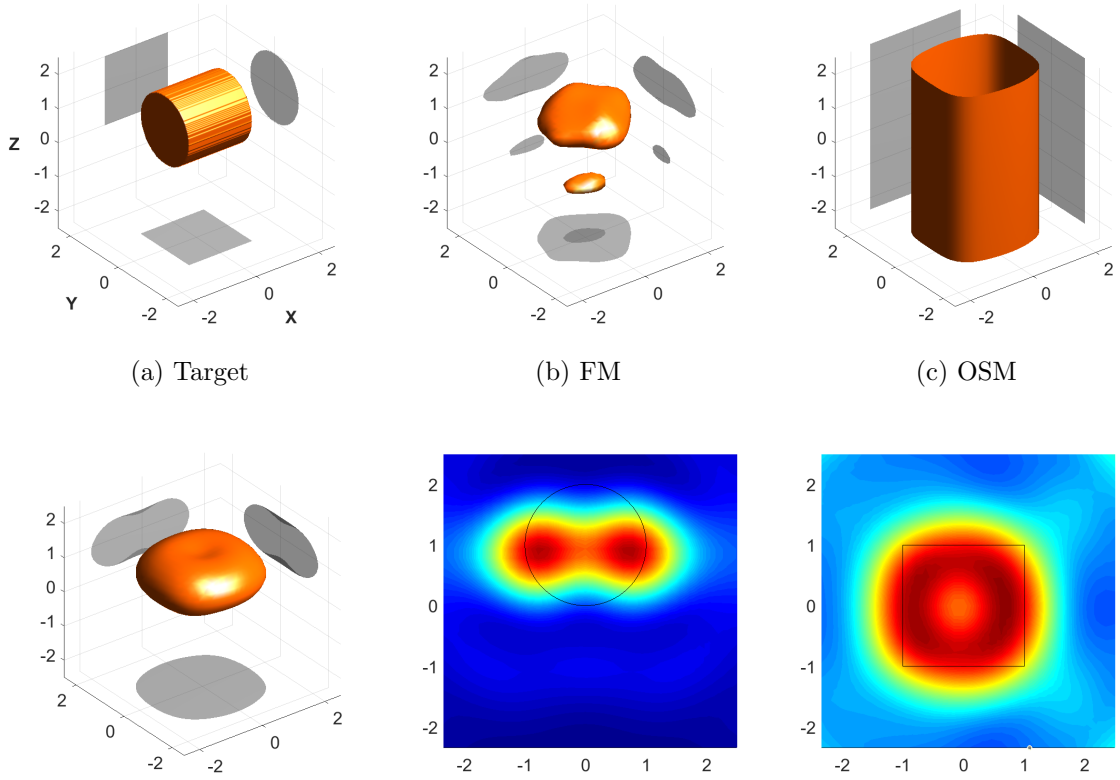

(a) Target (b) FM (c) OSM

(d) MOSM (e) $\mathcal{I}_{MOSM}$ on $\{x = 0\}$ (f) $\mathcal{I}_{MOSM}$ on $\{z = 0\}$

Figure 5: Reconstruction with Cylinder-PP dataset at 3 GHz.

(x, y)-plane.

6 Conclusion

We analyze a modified version of the orthogonality sampling method studied in [15] for both non-magnetic and magnetic cases for anisotropic Maxwell's equations. Comparing with its original version the modified OSM is proved to be applicable to more types of polarizations associated with the electromagnetic scattering data. We provide a validation of the modified OSM, its original version, and the factorization method for 3D experimental data from the Fresnel database. The results indicate that the modified OSM performs better than the other two methods and is a promising imaging approach in inverse scattering.

Acknowledgement. This work is partially supported by NSF grant DMS-1812693.

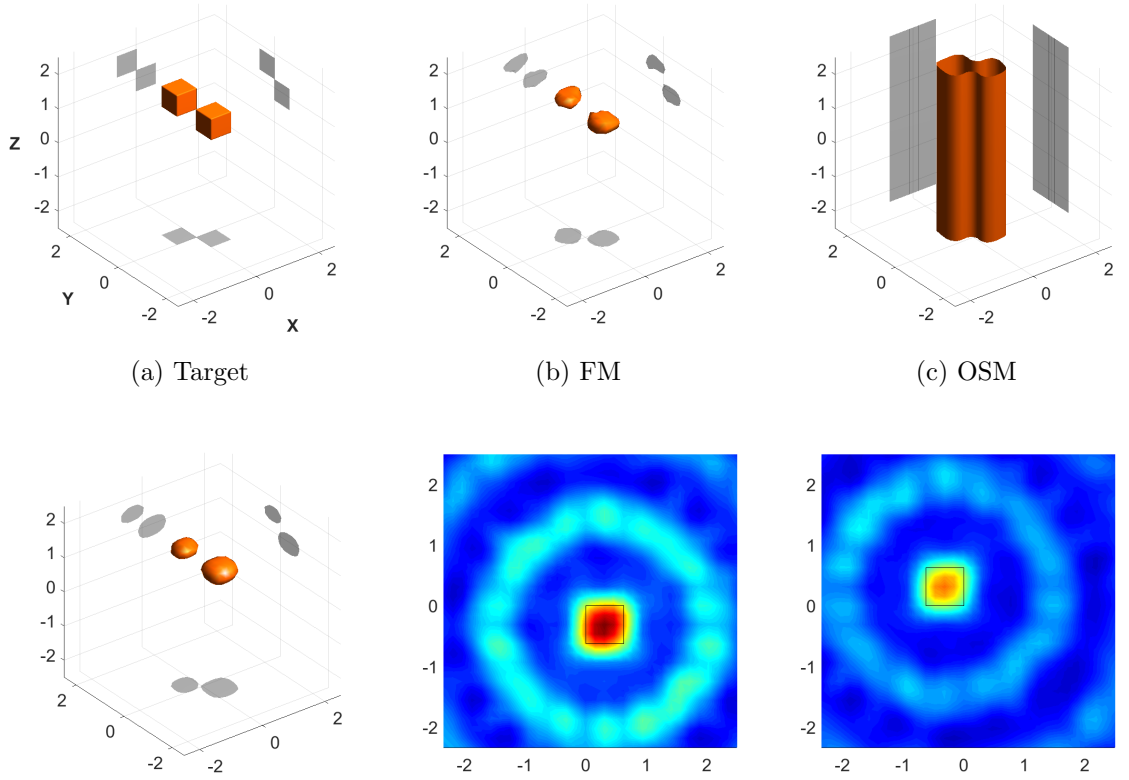

(a) Target (b) FM (c) OSM

(d) MOSM (e) $\mathcal{I}_{MOSM}$ on $\{z = 0.9375\}$ (f) $\mathcal{I}_{MOSM}$ on $\{z = 1.5625\}$

Figure 6: Reconstruction with TwoCubes-PP dataset at 7.5 GHz.

References

[1] C. Y. Ahn, S. Chae, and W.-K. Park. Fast identification of short, sound-soft open arcs by the orthogonality sampling method in the limited-aperture inverse scattering problem. *Appl. Math. Lett.*, 109:106556, 2020.

[2] M. Akinci, M. Cayoren, and I. Akduman. Near-field orthogonality sampling method for microwave imaging: Theory and experimental verification. *IEEE Trans. Microw. Theory Tech.*, 64:2489, 2016.

[3] F. Cakoni and D. Colton. *Qualitative Methods in Inverse Scattering Theory. An Introduction.* Springer, Berlin, 2006.

[4] F. Cakoni, D. Colton, and H. Haddar. *Inverse Scattering Theory and Transmission Eigenvalues.* SIAM, 2016.

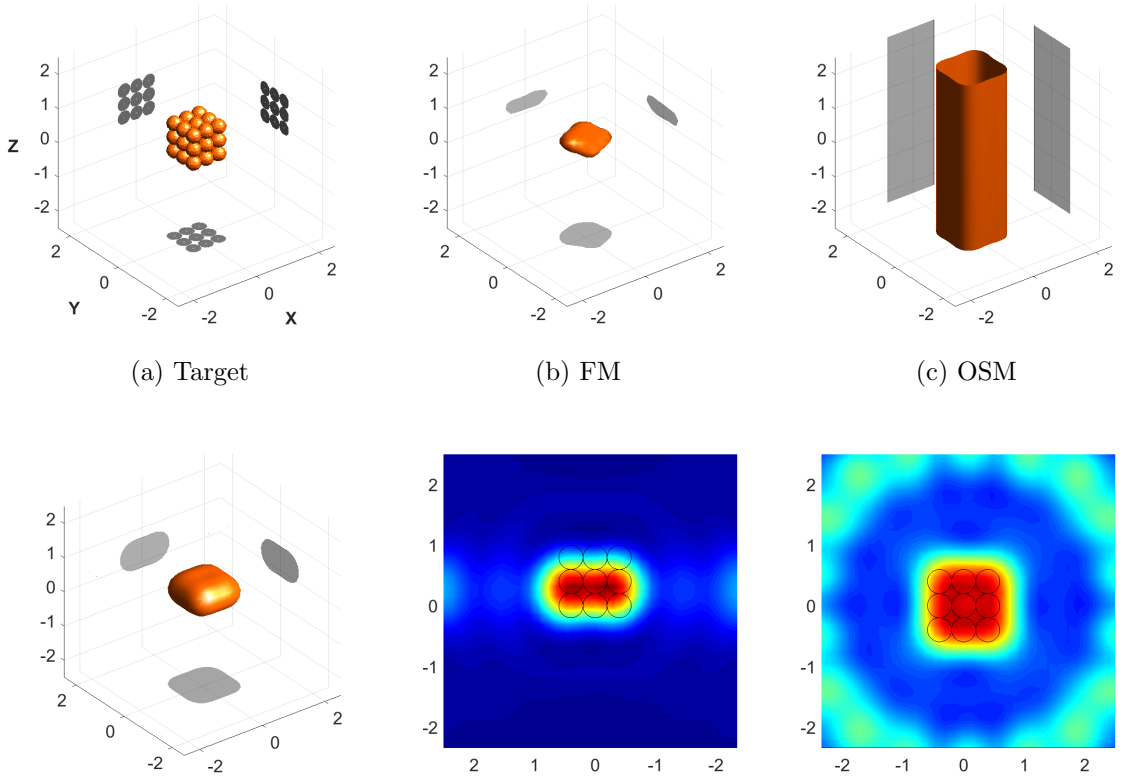

(a) Target (b) FM (c) OSM

(d) MOSM (e) $\mathcal{I}_{MOSM}$ on $\{y = 0\}$ (f) $\mathcal{I}_{MOSM}$ on $\{z = 0.3975\}$

Figure 7: Reconstruction with CubeSpheres-PP dataset at 4.75 GHz.

[5] F. Cakoni, D. Colton, and P. Monk. *The Linear Sampling Method in Inverse Electromagnetic Scattering*. SIAM, 2011.

[6] I. Catapano, L. Crocco, M. D'Urso, and T. Isernia. 3D microwave imaging via preliminary support reconstruction: testing on the Fresnel 2008 database. *Inverse Problems*, 25:024002, 2009.

[7] P. C. Chaumet and K. Belkebir. Three-dimensional reconstruction from real data using a conjugate gradient coupled dipole method. *Inverse Problems*, 25:024003, 2009.

[8] D. Colton, J. Coyle, and P. Monk. Recent developments in inverse acoustic scattering theory. *SIAM Review*, 42:396–414, 2000.

[9] D. Colton and A. Kirsch. A simple method for solving inverse scattering problems in the resonance region. *Inverse Problems*, 12:383–393, 1996.

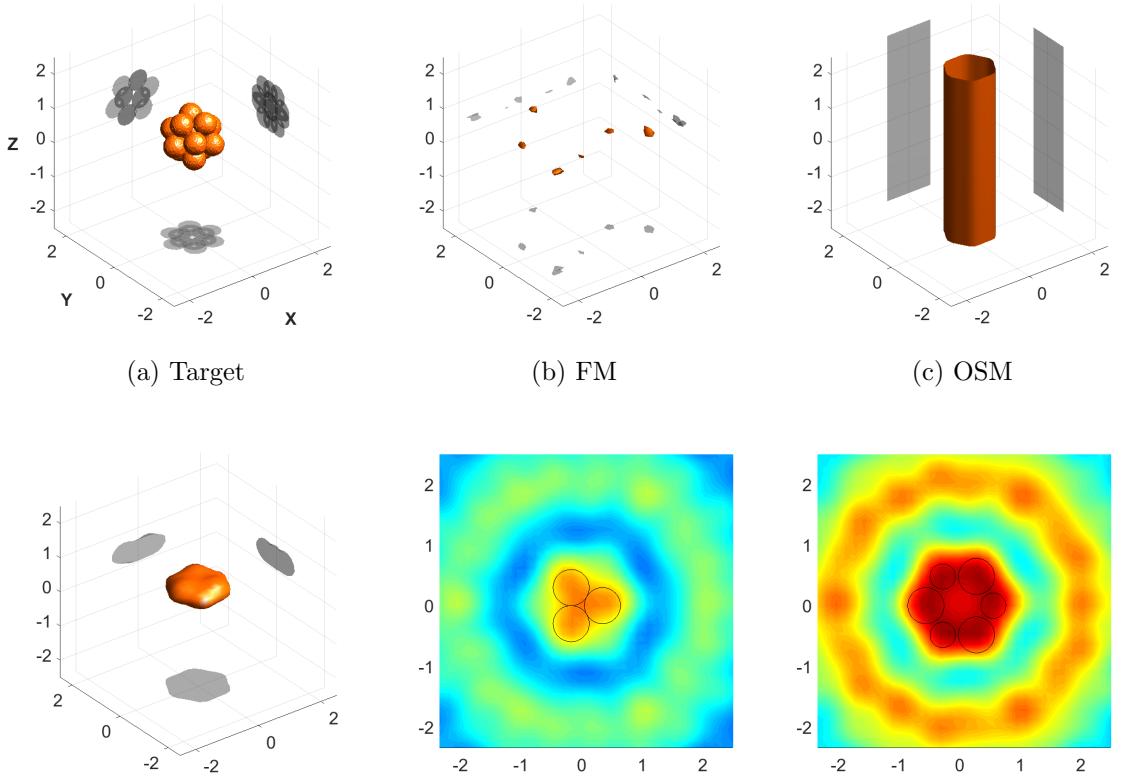

(a) Target (b) FM (c) OSM

(d) MOSM (e) $\mathcal{I}_{MOSM}$ on $\{z = 0\}$ (f) $\mathcal{I}_{MOSM}$ on $\{z = 0.3435\}$

Figure 8: Reconstruction with IsocaSphere-PP dataset at 5.75 GHz.

[10] D. Colton and R. Kress. *Inverse Acoustic and Electromagnetic Scattering Theory*. Springer, New York, 3rd edition, 2013.

[11] J. DeZaeytijd and A. Franchois. 3D quantitative microwave imaging from measured data with multiplicative smoothing and value picking regularization. *Inverse Problems*, 25:024004, 2009.

[12] J. M. Geffrin and P. Saboroux. Continuing with the Fresnel database: experimental set-up and improvements in 3D scattering measurements. *Inverse Problems*, 25:024001, 2009.

[13] R. Griesmaier. Multi-frequency orthogonality sampling for inverse obstacle scattering problems. *Inverse Problems*, 27:085005, 2011.

[14] H. Haddar. Analysis of some qualitative methods for inverse electromagnetic scattering problems. In *Bermudez de Castro A., Valli A. (eds) Computational Electro-*

magnetism. Lecture Notes in Mathematics, vol 2148, pages 191–240. Springer, Cham, 2014.

[15] I. Harris and D.-L. Nguyen. Orthogonality sampling method for the electromagnetic inverse scattering problem. *SIAM J. Sci. Comput.*, 42:B72–B737, 2020.

[16] M. Ikehata. Enclosing a polygonal cavity in a two-dimensional bounded domain from Cauchy data. *Inverse Problems*, 15:1231–1241, 1999.

[17] K. Ito, B. Jin, and J. Zou. A direct sampling method to an inverse medium scattering problem. *Inverse Problems*, 28:025003, 2012.

[18] S. Kang and M. Lambert. Structure analysis of direct sampling method in 3D electromagnetic inverse problem: near- and far-field configuration. *Inverse Problems*, 37:075002, 2021.

[19] A. Kirsch. Characterization of the shape of a scattering obstacle using the spectral data of the far field operator. *Inverse Problems*, 14:1489–1512, 1998.

[20] A. Kirsch. The factorization method for Maxwell's equations. *Inverse Problems*, 20:S117–S134, 2004.

[21] A. Kirsch. An integral equation approach and the interior transmission problem for Maxwell's equations. *Inverse Probl. Imaging*, 1:159–180, 2007.

[22] A. Kirsch and N.I. Grinberg. *The Factorization Method for Inverse Problems*. Oxford Lecture Series in Mathematics and its Applications 36. Oxford University Press, 2008.

[23] K. H. Leem, J. Liu, and G. Pelekanos. Two direct factorization methods for inverse scattering problems. *Inverse Problems*, 34:125004, 2018.

[24] M. Li, A. Abubakar, and P. M. van den Berg. Application of the multiplicative regularized contrast source inversion method on 3D experimental fresnel data. *Inverse Problems*, 25:024006, 2009.

[25] A. Litman and L. Crocco. Testing inversion algorithms against experimental data: 3D targets. *Inverse Problems*, 25:020201, 2009.

[26] P. Monk. *Finite Element Methods for Maxwell's Equations*. Oxford Science Publications, Oxford, 2003.

[27] D.-L. Nguyen. Direct and inverse electromagnetic scattering problems for bi-anisotropic media. *Inverse Problems*, 35:124001, 2019.

[28] W.-K. Park. Direct sampling method for retrieving small perfectly conducting cracks. *J. Comput. Phys.*, 373:648–661, 2018.

[29] W.-K. Park. Experimental validation of the factorization method to microwave imaging. *Results in Physics*, 17:103071, 2020.

[30] R. Potthast. A fast new method to solve inverse scattering problems. *Inverse Problems*, 12:731–742, 1996.

[31] R. Potthast. A study on orthogonality sampling. *Inverse Problems*, 26:074015, 2010.